

# Application of portable FTIR spectrometers for detecting greenhouse gas emissions of the megacity Berlin

F. Hase(1), M. Frey(1), T. Blumenstock(1), J. Groß(1), M. Kiel(1), R. Kohlhepp(2), G. Mengistu Tsidu(1,4), K. Schäfer(3), M. K. Sha(1), and J. Orphal(1)

(1) Karlsruhe Institute of Technology (KIT), Institute for Meteorology and Climate Research (IMK-ASF), Karlsruhe, Germany

(2) German Weather Service, Offenbach, Germany

(3) Karlsruhe Institute of Technology (KIT), Institute for Meteorology and Climate Research (IMK-IFU), Garmisch-Partenkirchen, Germany

(4) Department of Physics, Addis Ababa University, P.O.Box: 1176, Addis Ababa, Ethiopia

Correspondence to: Frank Hase (frank.hase@kit.edu)

## Abstract

Five portable Bruker EM27/SUN FTIR spectrometers have been used for the accurate and precise observation of column averaged abundances of CO<sub>2</sub> and CH<sub>4</sub> around the megacity Berlin. In the work by Frey et al., 2015, a calibration procedure is developed and applied to the set of spectrometers used for the Berlin campaign. Here, we describe the observational setup of the campaign and aspects of the data analysis, and we present the recorded time series of XCH<sub>4</sub> and XCO<sub>2</sub>. We demonstrate that the CO<sub>2</sub> emissions of Berlin can be clearly identified in the observations. A simple dispersion model is applied which indicates a total strength of the Berlin source of about 0.8 tons of CO<sub>2</sub> per second. In the electronic supplement of this work, we provide the measured dataset and auxiliary data. We hope that the model community will exploit this unique dataset for state-of-the art inversion studies of CO<sub>2</sub> and CH<sub>4</sub> sources in the Berlin area.

1

## 2 **1 Introduction**

3 The application of portable FTIR spectrometers for the observation of column-averaged CO<sub>2</sub>  
4 and CH<sub>4</sub> abundances holds great promises with respect to the quantification of sources and  
5 sinks of greenhouse gases on regional and smaller scales. Although in-situ measurements at  
6 the ground can be performed with unrivaled precision and accuracy, these measurements  
7 suffer from the fact that they detect local variations and so are heavily influenced by local  
8 contributions and by details of the vertical mixing. Use of in-situ measurements on different  
9 altitude levels (tall tower, aircraft) improves the representativeness considerably, but is a  
10 rather expensive approach. Current space based remote sensing observations are useful for the  
11 quantification of sources and sinks on continental scales, but still suffer from limited  
12 precision, limited density of observations, and biases related to details of atmospheric  
13 scattering properties. Ground-based observations using high-resolution laboratory  
14 spectrometers as performed by TCCON (Total Carbon Column Observing Network, Wunch  
15 et al., 2011) can provide column averaged abundances with reference precision and accuracy,  
16 but the number of sites is limited and the stations are not mobile. Portable FTIR spectrometers  
17 therefore are a very promising complement to current techniques, because they can probe  
18 larger sample volumes than in-situ and smaller scales than current space-based sensors or  
19 globally distributed ground-based remote sensing networks. In this work, we demonstrate the  
20 approach of using solar absorption spectra recorded with small low-resolution FTIR  
21 spectrometers at several sites distributed around a source region for an estimation of the  
22 encircled source strength.

23 The demonstration is based on a campaign we performed from June, 23, 2014 to July, 11,  
24 2014 around Berlin using five spectrometers. We decided to target Berlin for several reasons.  
25 Firstly, Berlin is a megacity, so we expect to measure detectable enhancements. Secondly, the  
26 city is relatively isolated, so that CO<sub>2</sub> emissions really can be attributed to Berlin. Thirdly, the  
27 flat topography is favorable, which supports the interpretation of the recorded data.  
28 Measurements were performed at five different stations around Berlin, four of them roughly  
29 located along a circle with a radius of 12 km around the city centre of Berlin. One instrument  
30 was positioned inside the Berlin motorway ring in Charlottenburg, somewhat closer to the city  
31 centre than the other instruments. A map with all sites is shown in figure 1. The coordinates  
32 and altitudes of the different stations are displayed in table 1. Due to somewhat unfavourable

1 weather conditions, we were able to perform simultaneous measurements at all sites only on  
2 10 days during the demonstration campaign. However, it should be noted that such  
3 spectrometers can be installed for longer periods of operation in weather-resistant shelters and  
4 operated automatically – in order to ~~from~~ form a permanent component of future monitoring  
5 systems.

6

7 Due to the long lifetimes of CO<sub>2</sub> and CH<sub>4</sub>, each individual source contribution is a weak  
8 signal superimposed on the average column-averaged background abundance. Therefore,  
9 ensuring a common calibration of all involved spectrometers and demonstrating their  
10 instrumental stability is of utmost importance for the proposed method. In Frey et al., 2015, a  
11 rigorous calibration procedure for the EM27/SUN spectrometer is developed and is  
12 exemplified using the set of portable spectrometers which we used for the Berlin campaign.  
13 This calibration procedure involved pre- and after campaign measurements, thereby proving  
14 unambiguously the excellent instrumental stability of the devices.

15

## 16 **2 Observational setup, weather, prevailing winds and auxiliary** 17 **measurements**

18 Each site was equipped with an EM27/SUN spectrometer including a solar tracker, a GPS  
19 sensor used for accurate timekeeping, and a MHB-382SD data logger for pressure,  
20 temperature and relative humidity. The measurement procedures (scan speed, resolution,  
21 numerical apodisation, etc) applied during the campaign were chosen identical to those  
22 applied for the calibration measurements.

23

24 In table 2, we collect the main characteristics of each measurement day. We list the number of  
25 observations available at each site, and deduce a daily quality flag according to the overall  
26 data availability. Furthermore, the wind speeds and prevailing wind directions in the boundary  
27 layer are provided. The best measurement days with measurements during throughout most of  
28 the day (solar elevation angle > 20 deg) were June, 27, July, 3, and July, 4. During these days,  
29 prevailing winds were from the West (and South). Wind speeds were moderate in the range of  
30 5 to 8 knots. Note that although not very well covered, the set of observations includes a

1 Sunday (July, 6), which is an interesting aspect, as a different temporal pattern and overall  
2 strength of emissions is expected on a Sunday than during a working day.

3

4 A very important auxiliary information required for the proper estimation of a source strength  
5 is the development of the boundary layer height during each day of observations. IMK-IFU  
6 performed continuous ceilometer measurements of the boundary layer height during the  
7 whole campaign period. The measurements were performed in Berlin Neukölln (52.4895 N,  
8 13.4309 E), 2.5 km to the southeast from the city center. The **applied** ceilometer CL51 from  
9 Vaisala GmbH, Hamburg, Germany, is an eye-safe commercial mini-lidar system.  
10 Ceilometers detect **originally initially** the cloud height, but special software provides routine  
11 retrievals of up to 5 lifted layers from vertical profiles (vertical gradient) of laser backscatter  
12 density data (Münkel, 2007). In the absence of low clouds and precipitation and during  
13 scattered clouds, this measurement method estimates boundary layer height fairly well. The  
14 CL51 detects convective layer depths exceeding 2000 m and nocturnal stable layers down to  
15 50 m. The measurements results agree well with those which are determined from profiles of  
16 relative humidity and virtual potential temperature measured by radiosonde (location of  
17 strong height gradient of aerosol backscatter density and relative humidity as well as  
18 temperature inversion, see Emeis et al. , 2012). But radiosondes which are launched routinely  
19 twice per day only do not provide sufficient information. Figure 2 shows the ceilometer  
20 results for June, 27: the developing boundary layer can be **nicely clearly** seen, reaching an  
21 altitude of about 2200 m in the late afternoon. In the case of airborne particles it could be  
22 shown earlier that boundary layer information as detected continuously by ceilometers  
23 enables the determination of near-surface concentrations from column density data (Schäfer et  
24 al., 2008).

25

### 26 **3 The XH<sub>2</sub>O, XCO<sub>2</sub> and XCH<sub>4</sub> time series**

27 The analysis of the trace gases from the measured spectra has been performed as described by  
28 Gisi et al., 2012, and Frey et al., 2015. Because the distances between the sites are about 25  
29 km or less, a common pressure-temperature profile has been used for the analysis at all sites.  
30 The pressure records of the MHB-382SD devices have been used to set the ground pressure  
31 values of the model atmosphere, and an intraday variability of the ground pressure and the  
32 temperature profile has been taken into account in the analysis of the spectra. For the

1 construction of the temperature profiles, we utilize the NCEP model noon profiles provided  
2 by the Goddard automailer system and radiosonde data provided by the meteorological  
3 observatory Lindenberg. We take the NCEP data as the starting values and overlap a linear  
4 ascent during the day, which is the temperature difference between the 12 am and 6 pm sonde  
5 data, for the lowermost height levels (below 4 km altitude). For the height levels above 4 km  
6 we take the original NCEP noon data, as the change during the day is negligible.

7  
8 Solar absorption spectral observations in the near infrared offer the potential of measuring  
9 column-averaged dry air mole fractions with excellent precision and accuracy. This is owed to  
10 the facts that (1) scattering of photons into the line-of-sight is a negligible process and that (2)  
11 absorption bands of molecular oxygen are covered, so the column amount of oxygen can be  
12 derived from the same spectrum. Because the dry air mole fraction of molecular oxygen is  
13 nearly invariable, the column-averaged dry air mole fraction of the target gases can be derived  
14 from the ratio of the observed target gas columns and the oxygen column. This approach  
15 significantly reduces the impact of various error sources on the final results, because these  
16 typically affect both the target gas columns and the oxygen reference column (Wunch et al.,  
17 2011). Moreover, the amount of dry air deduced from the spectral information can be  
18 compared with the ground pressure measured with a barometer. Note that the barometer  
19 records the total ground pressure including the pressure exerted by the water vapour column.  
20 However, this small contribution to the pressure can be taken into account in the comparison,  
21 because the water vapour column can also be derived from the observed spectrum. Figure 3  
22 shows the time series of the total ground pressure (derived from the average of the continuous  
23 barometer measurements performed with the MHB-382SD devices at all five sites) in  
24 comparison to the total ground pressures calculated from the spectral measurements (taking  
25 into account the water vapour contribution). The pressure values from the spectral  
26 measurements follow closely the variable ground pressure and the agreement between  
27 different stations is excellent. A least squares fit to the barometer data suggests a common  
28 calibration factor of 0.9713 for the spectroscopic measurements, which has been applied in  
29 the figure. This result is in excellent agreement with the calibration factor found by Frey et  
30 al., 2015 (0.9700) and Klappenbach et al., 2015 (0.9717).

31

1           Figure 4 shows the observed time series of H<sub>2</sub>O dry air mole fractions. As expected,  
2 H<sub>2</sub>O ~~is varying~~ varies considerably - by about a factor of three - over the campaign period. On  
3 the other hand, the agreement between the stations is surprisingly good. This demonstrates the  
4 uniform character of the selected area, especially the absence of localized dominating sources  
5 of atmospheric humidity, which would induce larger differences between the stations. Finally,  
6 as the main contribution to the H<sub>2</sub>O total column originates from the boundary layer, this  
7 finding supports the assumption that the boundary layer across the whole probed area is well  
8 ventilated.

9

10 Figures 5 and 6 show the XCO<sub>2</sub> and XCH<sub>4</sub> values, respectively, as observed by all  
11 spectrometers. The dominating synoptic variations which are common to all sites occur on  
12 timescales of several days. These variations in the order of one per cent peak-to-peak are due  
13 to the changing tropopause altitude and advection of air masses with different trace gas  
14 concentrations. In addition, the time series reveal intraday variability in the order of 0.5 % or  
15 less, which is variable from day to day, but also very similar in each individual data record.  
16 We assume that these variations result from a superposition of real variability and artefacts of  
17 the retrieval. During most of the observation days, a decrease of XCO<sub>2</sub> is found, which is  
18 what would be expected as a result of photosynthetic activity during a sunny day (high  
19 insolation being an obvious selection bias of solar absorption observations). On the other  
20 hand, variations symmetric around noon are particularly striking during a couple of days,  
21 mainly in the case of CH<sub>4</sub>. It is plausible to assume an airmass-dependent retrieval biases as a  
22 cause of these variations. We detailed in the first part of this work that we attempted to  
23 remove this artefact by applying an a-posteriori airmass-dependent correction. However, the  
24 observed bias will be comprised of two contributions: one contribution resulting from forward  
25 model errors (e.g. wrong line broadening parameters) - this tends to be a systematic feature  
26 and can be removed by the global correction we applied - and a second contribution due to the  
27 smoothing error of the retrieval. The column sensitivity of the scaling retrieval is a function of  
28 airmass, and so is the smoothing error. As described in the first part of this work, we used  
29 constant a-priori profile shapes in the retrievals, while the actual atmospheric profiles are  
30 variable. This gives rise to airmass-dependent artefacts which are variable from day to day.  
31 Finally, on top of this variable background, subtle differences between individual  
32 observations can be detected: these are typically of the order of 1 to 2 per mil and it is

1 tempting to assume that these are caused by local emission contributions. For illustration,  
2 figure 7 shows the  $XCH_4$  and  $XCO_2$  values observed during June, 27. Southerly winds  
3 prevailed during that day, and indeed the  $XCO_2$  values observed in Heiligensee in the  
4 Northwest of Berlin are elevated. It is important to note that although the emission signals  
5 tend to be smaller than the observed intraday variability, enhancements as small as 0.5 per mil  
6 are noticeable. This is possible because the detection of an enhancement can be based on the  
7 differences between the column-averaged mole fractions observed at different sites, if these  
8 are superimposed on a smoothly varying background traced by the observations of several  
9 upstream stations. This situation is realized if all sites observe similar advected larger scale  
10 variations. Note that at a given time during the day all sites perform measurements under  
11 nearly the same solar elevation angle and quite similar atmospheric conditions (atmospheric  
12 vertical profile shapes of trace gases). This reduces significantly retrieval biases between the  
13 stations, especially if the interpretation of the collected data is mainly based on differences  
14 between simultaneous observations of upstream and downstream stations. In detail, the  
15 observed  $XCH_4$  enhancements differ from the  $XCO_2$  enhancements, which is expected due to  
16 different sources. Moreover, the background of the  $XCH_4$  seems less well defined and more  
17 variable. This meets the expectation: due to the likely presence of rural  $CH_4$  sources around  
18 the conurbation area encircled with the stations and due to the stronger contrast between  
19 tropospheric and stratospheric mixing ratios of  $CH_4$  higher variability is expected in the  $XCH_4$   
20 background field than in case of  $XCO_2$ . We feel that a sensible investigation of our  $XCH_4$   
21 observations would require a state-of-the-art high-resolution inversion model and we hope  
22 that the datasets made available in the electronic supplement of this work will be exploited in  
23 depth by the inverse model community. Using a simple dispersion model, we will in the  
24 following focus on a more specific interpretation of the observed  $XCO_2$  enhancements. In the  
25 next section, we describe the main characteristics of the dispersion model. In section 5 we  
26 compare observations and model predictions.

27

28

#### 29 **4 Setup of a simple dispersion model**

30 For a prediction of the differences in  $XCO_2$  between different sites we have created a simple  
31 dispersion model. Within this modelling scheme, the Berlin source is mapped into a  
32 schematic area source spanned by 5 neighbouring rectangles, which contribute to the total

1 source strength. The central rectangle reflects the city center, the four remaining rectangles  
2 reflect Charlottenburg and Spandau areas (western box), Reinickendorf and Pankau areas  
3 (northern box), Marzahn-Hellersdorf and Treptow-Köpenick areas (eastern / south-eastern  
4 box), and the Tempelhof-Schöneberg area (southern box). The geographical coordinates of  
5 each box and the percentage contribution to the total emission are listed in table 3. The spatial  
6 extent and contribution of each box have been ~~inspired by~~ adjusted according to informations  
7 on population and traffic density provided by the bureau of statistics of Berlin-Brandenburg  
8 (<http://www.stadtentwicklung.berlin.de>).

9

10 The dispersion model uses analysed hourly horizontal wind fields from COSMO-DE, the  
11 convective-scale regional component of the numerical weather prediction system of the  
12 German Weather Service DWD (Baldauf et al., 2011). Due to the fact that we assume a  
13 distributed source region, we do not apply the COSMO wind field at full resolution, which is  
14 in the order of 2.8 x 2.8 km, but use only 5 COSMO hourly wind profiles distributed over the  
15 observation area (in the center and the NW, NE, SW, SE corners of a square centered on  
16 Berlin with an edge length of about 20 km) and interpolate the winds between these reference  
17 wind profiles linearly along time and - assuming a Shepard inverse distance weighting with a  
18 power of two (Shepard, 1968) - in a horizontal plane.

19

20 The model is based on a strict Lagrangian perspective. It does not use a model grid,  
21 but instead transports emitted ~~“molecules”~~ particles according to the interpolated winds at  
22 their current locations. The generation rate of the ~~“molecules”~~ particles is proportional to the  
23 source strength, they are created at the ground level within one of the five emission regions  
24 described before. For each creation act, the region is selected by a random generator in  
25 accordance with the assumed contribution of the region, the starting position within the  
26 selected area is again chosen randomly. Within a selected region, the probability of emission  
27 is equal for each area element; we do not attempt to resolve sources on a scale smaller than  
28 the source region.

29

30 Concerning the vertical transport, a fast mixing on timescales of ~10 minutes across the whole  
31 boundary layer is assumed. This is realized in the model by introducing a fast erratic diffusion

1 of each “molecule” along the vertical axis. The altitude limit of the model boundary layer is  
2 for each day chosen in accordance with ceilometer measurements. Fast fluctuations of the  
3 boundary layer thickness detected by the ceilometer are neglected, instead the individual  
4 overall development of the boundary layer height during each day is approximated using  
5 piecewise linear fits.

6

7 Finally, the detection of “~~molecules~~” particles is emulated by checking whether the  
8 “molecule” is inside a cylinder which wraps the line of sight of one of the observation sites. It  
9 should be noted that due to the daily apparent motion of the sun in the sky, the position of this  
10 cylinder is quite variable. If we assume a boundary layer thickness of 1500 m and start and  
11 end of observations at a solar elevation angle of 20 degree, then the top surface of the cylinder  
12 is shifted by 8 km westwards during the day, which is not negligible in comparison to the  
13 extent of the assumed source regions. Therefore, the line-of-sight used for the detection  
14 condition is updated in the model according to the astronomical conditions.

15

16 The simulation period starts at midnight. In each time step (1 sec), a “molecule” is  
17 emitted and all existing “~~molecules~~” particles are transported. During daytime, as long as the  
18 solar elevation exceeds 20°, the number of detected ~~molecules~~ particles at each observation  
19 site is determined in intervals of 450 sec. Typically, depending on wind speed, 20 000 to 40  
20 000 “~~molecules~~” particles are traced at a given time (each emitted “molecule” is followed for  
21 up to a distance of 40 km from the Berlin center). The simulation run for each day is repeated  
22 500 times and the results averaged to achieve a negligible statistical noise in the number of  
23 detection counts. Note that the model does not take into account emissions from the previous  
24 day. Typically, these aged emissions have left the region of interest before, but occasionally -  
25 if the wind speed is very low - it might happen that they reside for longer than 6 hours in the  
26 observed area, or may return from outside the modelled area if the wind direction is changing.  
27 No attempt is made in the dispersion calculation to include the variable advected XCO<sub>2</sub>  
28 background, it only predicts the enhancements at each observation site due to the daily  
29 emissions of the local Berlin source.

30

## 1 **5 Comparison of predicted and observed time series**

2 In the following, we compare the XCO<sub>2</sub> measurements with results from the dispersion model  
3 for the three most favourable observation days. For all days, the Berlin CO<sub>2</sub> source strength  
4 was fixed to a plausible value of 800 kg CO<sub>2</sub> per second. The source strength was kept  
5 constant during the day, although one would certainly expect considerable intraday variability  
6 for different kinds of contributions, e.g. traffic peaking at around 8 am and 5 pm (local time).  
7 Figures 8 to 10 show the observational and model results for June, 27, July, 3, and July, 4. For  
8 the first two days, the model enhancements are shown superimposed on a smooth polynomial  
9 background, which is reasonably well defined by the observations of the upstream stations.  
10 During the third day, July, 4, it is more difficult to estimate a smooth background level, as all  
11 stations, including the upstream stations, observe considerable variability. Therefore, for this  
12 day the predicted enhancements are shown superimposed on a constant 390 ppm background  
13 level.

14

15 The model prediction for June, 27, is of acceptable quality. The enhancements before noon  
16 observed first in Charlottenburg and afterwards in Heiligensee are well captured. The peak at  
17 0.35 day fraction observed in Heiligensee, is much sharper than the model prediction and  
18 indicates a significant contribution of a localised source smaller than the assumed emission  
19 regions. Southerly winds prevailed during the day, so this source is probably located in model  
20 region 1. Indeed, the heat and power generating coal-fired plant Reuter West operated by  
21 Vattenfall AB with a peak thermal power of 774 MW (Ref:  
22 <http://kraftwerke.vattenfall.de/powerplant/reuter-west>) is located in this region and is the  
23 likely source of the observed emissions. Afterwards, the model predicts elevated values for  
24 Heiligensee until around noon, which is in good agreement with the observations, but it fails  
25 to predict the final enhancement observed in Heiligensee after noontime.

26

27 For July, 3, the enhancements are smaller than those observed during June, 27. Still, the  
28 undulations predicted by the model are detectable in the Lindenberg time series reasonably  
29 well, although the first two peaks are underestimated and appear delayed by about half an  
30 hour. The final increase towards the third peak observed in the afternoon is nicely reproduced.  
31 The model predicts slightly higher values for Mahlsdorf than for Heiligensee and Lichtenrade,  
32 which is not supported by the observations, which instead indicate repeated peaks in the

1 Heiligensee and Lichtenrade timeseries. Westerly winds were prevailing during that day, so  
2 for the station Lichtenrade emissions from Potsdam (not included in the model) are likely to  
3 contribute.

4 For July, 4, the observed XCO<sub>2</sub> values are quite variable. An M-shaped disturbance extending  
5 over 5 hours and observed at all stations before noon is most prominent feature. Southerly  
6 winds prevailed near ground and southwesterly winds in the free troposphere. While a similar  
7 shape is observed at all stations, there is a clear time lag of about 45 minutes between the  
8 occurrence of this disturbance between the upstream stations (Lichtenrade and  
9 Charlottenburg) and the downstream stations (Heiligensee and Lindenberg). This time lag  
10 agrees well with the delay expected for the advection of a disturbance in the background  
11 XCO<sub>2</sub> signal at a wind speed of about 13 Kn across a distance of about 20 km between the  
12 sites. The variations between the stations are too strong to allow a judgement concerning the  
13 model prediction of a 0.5 ppm enhancement at Heiligensee and Charlottenburg.

14

15 Figure 11 shows the MACC ([Monitoring Atmospheric Composition & Climate project](#))  
16 prediction for XCO<sub>2</sub>. A closer examination of the previous development of the XCO<sub>2</sub> field  
17 according to MACC indicates that the complex structure in the XCO<sub>2</sub> field around Berlin  
18 during that day are possibly the result of an entrainment of emissions from Western Germany  
19 and further sources nearer to Berlin. The example of July, 4, demonstrates the limitations of a  
20 simple dispersion model which takes into account only the local source. A comprehensive  
21 exploitation of the information contained in the kind of measurements presented here would  
22 require state-of-the-art inverse modelling allowing for a resolved local source distribution  
23 nested into a much wider model area. Such a model configuration would include a reasonable  
24 description of variations due to advected XCO<sub>2</sub> contributions from outside the model area and  
25 associated larger-scale variations of column averaged abundances.

26

## 27 **6 Dataset provided in the Supplement**

28 In the electronic supplement of this work, we provide the complete set of quality-filtered  
29 XCH<sub>4</sub> and XCO<sub>2</sub> observations collected during the campaign at all stations. The quality filter  
30 is based on the quality of the interferograms (average value and fluctuation of the DC value).  
31 For each site, we provide the apparent solar elevation angle of the measurement, the retrieved

1 total column amount of H<sub>2</sub>O and the XCH<sub>4</sub> and XCO<sub>2</sub> calibrated with respect to TCCON and  
2 corrected for the systematic spurious air mass dependence (column-averaged dry air mole  
3 fractions in ppm). In separate tables, we provide the a-priori profile shapes of CH<sub>4</sub> and CO<sub>2</sub>  
4 used for the scaling retrieval on the 49 model levels of the retrieval code (dry air mole  
5 fractions in ppm) and the averaging kernels matrices of dimension 49 x 49 for different solar  
6 zenith angles. These auxiliary data enable the user to estimate the smoothing error of the  
7 column-averaged abundances, especially the impact of the actual profile shape on XCH<sub>4</sub> and  
8 XCO<sub>2</sub>. If the user wants to include the smoothing characteristics of the remote sensing  
9 observations in the comparison between observations and assimilation model we suggest  
10 including the kernel convolution directly in the model predictor. [In addition to the FTIR data,](#)  
11 [the electronic supplement contains the results derived from the ceilometer observations in](#)  
12 [both tabulated and graphical form.](#)

13

## 14 **7 Summary and Outlook**

15 We presented measurements of column averaged abundances of CH<sub>4</sub> and CO<sub>2</sub> recorded with  
16 five portable FTIR spectrometers during a measurement campaign of three weeks duration  
17 around Berlin in summer 2014. The results demonstrate that an array of well-calibrated,  
18 ground-based FTIR spectrometers allow the reliable detection of XCH<sub>4</sub> and XCO<sub>2</sub>  
19 enhancements due to local emissions in the range of one per mil. Application of a simple  
20 dispersion model indicates that the observations are compatible with an assumed source  
21 strength in the order of 800 kg CO<sub>2</sub> /s for the megacity Berlin. We believe that arrays formed  
22 with such spectrometers would be a very useful complement to existing in-situ and remote-  
23 sensing measurements for the quantification of sources and sinks of CH<sub>4</sub> and CO<sub>2</sub> on regional  
24 scales. We expect that a comprehensive inversion of local source contributions to the  
25 observed column averaged abundances will require state-of-the art nested model approaches  
26 which include a proper description of the variable advected background contributions. Such  
27 model studies could also be of great value for the design of monitoring networks (density and  
28 locations of stations) based on portable FTIR spectrometers.

29

## 30 **Acknowledgements**

31

1 We acknowledge support by the ACROSS research infrastructure of the Helmholtz  
2 Association.

3

4 We thank the National Center for Environmental Prediction (NCEP) for providing  
5 atmospheric temperature profiles via the Goddard Auto mailer system.

6

7 We acknowledge the availability of XCO<sub>2</sub> maps from MACC-III. MACC-III is a  
8 Coordination & Support Action (2014-2015) funded by the European Union under the  
9 Horizon 2020 Programme, coordinated by the European Centre for Medium-Range Weather  
10 Forecasts and operated by a 36-member consortium. Further project details can be found at  
11 <http://www.gmes-atmosphere.eu>. Andre Butz kindly prepared the plot based on MACC-III  
12 data.

13

14 We are very thankful for the successful cooperation during the measurement campaign  
15 “Berlin Air quality and Ecosystem Research: Local and long-range Impact of anthropogenic  
16 and Natural hydrocarbons” (BAERLIN2014), and especially the coordinators Boris Bonn and  
17 Erika von Schneidmesser, Institute for Advanced Sustainability Studies e.V., Potsdam,  
18 Germany.

19

20 We thank the German Weather Service (DWD) for providing the COSMO-DE analysis data  
21 which were used for the wind profiles in the dispersion model.

22

23 We acknowledge support by Deutsche Forschungsgemeinschaft and Open Access Publishing  
24 Fund of the Karlsruhe Institute of Technology.

25

26

27

## 1 **References**

- 2 Baldauf, M., A. Seifert, J. Förstner, D. Majewski, M. Raschendorfer, T. Reinhardt:  
3 Operational Convective-Scale Numerical Weather Prediction with the COSMO Model:  
4 Description and Sensitivities, *Mon. Wea. Rev.*, 139/12, 3887-3905, 2011, doi:  
5 10.1175/MWR-D-10-05013.1.
- 6 Emeis, S., Schäfer, K., Münkel, C., Friedl, R., and Suppan, P.: Evaluation of the interpretation  
7 of ceilometer data with RASS and radiosonde data, *Bound-Lay. Meteorol.*, 143, 25–35, 2012.
- 8 Frey, M., F. Hase, T. Blumenstock, J. Groß, M. Kumar Sha, M. Kiel, R. Kohlhepp, G.  
9 Mengistu Tsidu, K. Schäfer, and J. Orphal: ~~Use of portable FTIR spectrometers for detecting~~  
10 ~~greenhouse gas emissions of the megacity Berlin — part 1: instrumental line shape~~  
11 ~~characterisation and calibration of spectrometers~~ Calibration and instrumental line shape  
12 characterisation of a set of portable FTIR spectrometers for detecting greenhouse gas  
13 emissions, submitted to AMTD, 2015.
- 14 Gisi, M., Hase, F., Dohe, S., Blumenstock, T., Simon, A., and Keens, A.: XCO<sub>2</sub>-  
15 measurements with a tabletop FTS using solar absorption spectroscopy, *Atmospheric*  
16 *Measurement Techniques*, 5, 2969–2980, doi:10.5194/amt-5-2969-2012, 2012.
- 17 Klappenbach, F., M. Bertle, J. Kostinek, F. Hase, T. Blumenstock, A. Agusti-Panareda, M.  
18 Razingier and A. Butz: Accurate mobile remote sensing of XCO<sub>2</sub> and XCH<sub>4</sub> latitudinal  
19 transects from aboard a research vessel, submitted to AMTD, 2015.
- 20 Münkel, C.: Mixing height determination with lidar ceilometers - results from Helsinki  
21 Testbed, *Meteorol. Z.*, 16, 451-459, 2007.
- 22 Schäfer, K., Harbusch, A., Emeis, S., Koepke, P., and Wiegner, M.: Correlation of aerosol  
23 mass near the ground with aerosol optical depth during two seasons in Munich. *Atmos.*  
24 *Environ.*, 42, 18, 4036-4046, 2008.
- 25 Shepard, D.: Proceedings of the 1968 ACM National Conference. pp. 517–524, 1968,  
26 doi:10.1145/800186.810616.
- 27 Wunch, D., G.C. Toon, J.-F.L. Blavier, R.A. Washenfelder, J. Notholt, B.J. Connor, D.W.T.  
28 Griffith, V. Sherlock, P.O. Wennberg. The Total Carbon Column Observing Network. *Phil.*  
29 *Trans. R. Soc. A* , 2011, 369, doi:10.1098/rsta.2010.0240.
- 30

1

site	latitude [°]	longitude [° E]	altitude [m]
Mahlsdorf	52.486	13.589	39.0
Charlottenburg	52.505	13.302	47.7
Heiligensee	52.622	13.228	34.5
Lindenberg	52.601	13.519	63.3
Lichtenrade	52.391	13.392	44.8

2

3 Table 1. Geographical coordinates and altitudes of the measurement sites around Berlin. The  
4 coordinates were derived using GPS sensors. The reported altitudes result from combining  
5 time-averaged GPS measurements which were repeatedly performed at Mahlsdorf and  
6 average differences between the time series of ground pressures recorded at each site.  
7 Excellent agreement with topographic data provided on the website <http://www.wieweit.net>  
8 are found.

9

1

date JJMMDD	# observations	quality	wind speed (kn)	wind direction
140626 (Th)	76 / 70 / 89 / 28 / 116	+	2 ... 4	NNE
140627 (Fr)	273 / 233 / 237 / 186 / 182	+++	5	SSW ... SSE
140628 (Sa)	0 / 37 / 0 / 0 / 0	o	7	SSW
140701 (Tu)	203 / 189 / 158 / 122 / 224	++	8	W
140702 (We)	106 / 128 / 92 / 76 / 129	+	9	W
140703 (Th)	316 / 358 / 320 / 354 / 357	+++	7	W
140704 (Fr)	545 / 509 / 545 / 652 / 511	++++	7	SW ... S
140705 (Sa)	0 / 93 / 0 / 0 / 0	o	5	SSW ... SSE
140706 (Su)	329 / 265 / 346 / 252 / 385	++	5	W ... SW
140707 (Mo)	10 / 74 / 28 / 98 / 130	+	8	SE ... NW
140708 (Tu)	0 / 21 / 0 / 0 / 0	o	6	NE ... E
140709 (We)	35 / 29 / 40 / 0 / 10	o	6 ... 10	E ... SSW
140710 (Th)	248 / 306 / 411 / 188 / 245	++	6...12...6	NE ... E
140711 (Fr)	257 / 248 / 212 / 243 / 253	+	8	NE

2

3

4 Table 2. Summary of all measurement days: number of observations at each site (Mahlsdorf,  
5 Charlottenburg, Heiligensee, Lindenberg, Lichtenrade), overall quality ranking of each day  
6 according to number of available observations and temporal coverage, ground wind speed and  
7 direction.

1

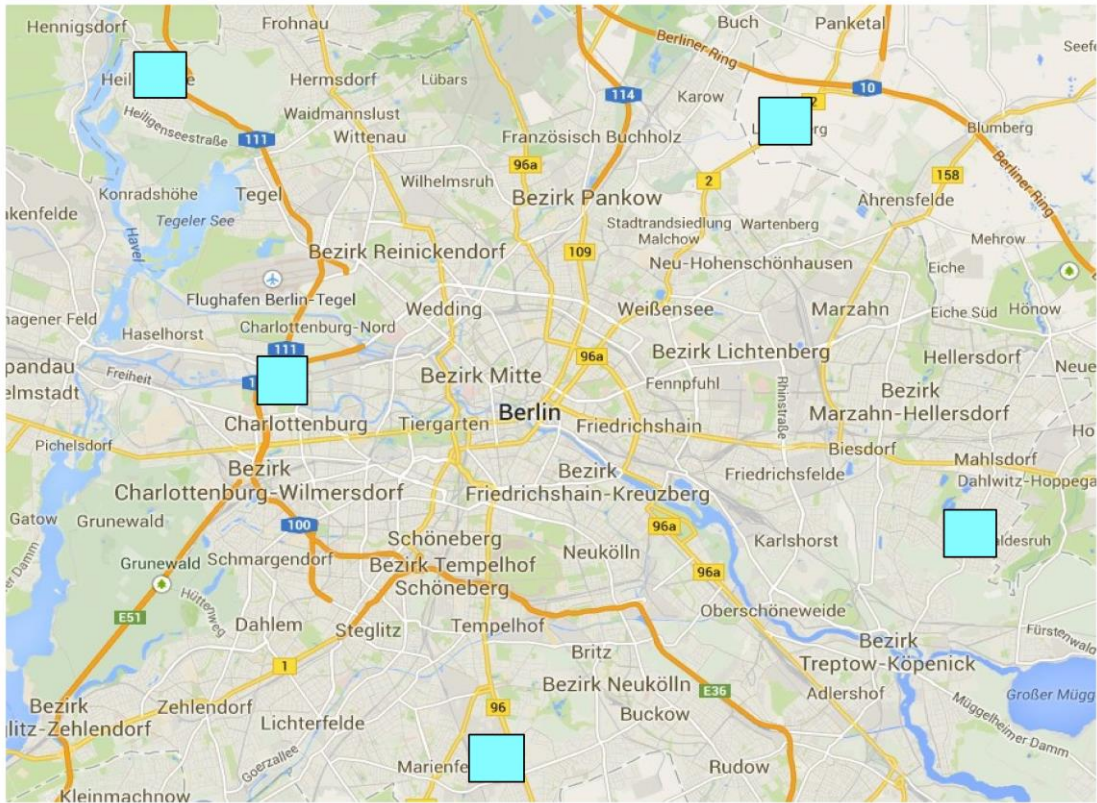
Box ID	area	NW corner	SE corner	% contribution
1	Charlottenburg and Spandau	52.5677 13.0753	52.5159 13.2550	25
2	Tempelhof-Schöneberg	52.4657 13.2304	52.3800 13.4275	15
3	Marzahn-Hellersdorf and Treptow-Köpenick	52.5531 13.4502	52.3927 13.6316	10
4	Reinickendorf and Pankau	52.6302 13.3046	52.5472 13.4721	10
5	city center	52.5472 13.2550	52.4657 13.4502	40

2

3 Table 3. The five emission regions used in the dispersion model.

4

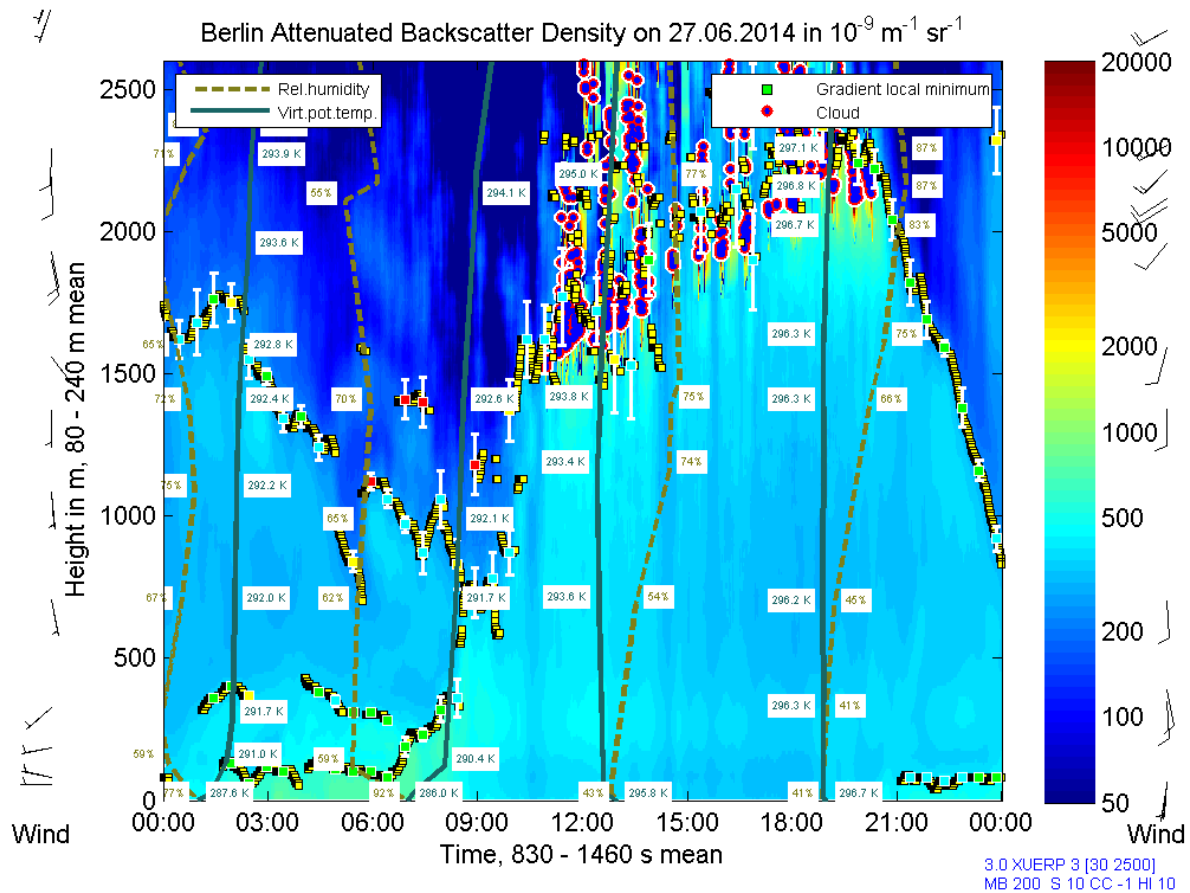
5



1

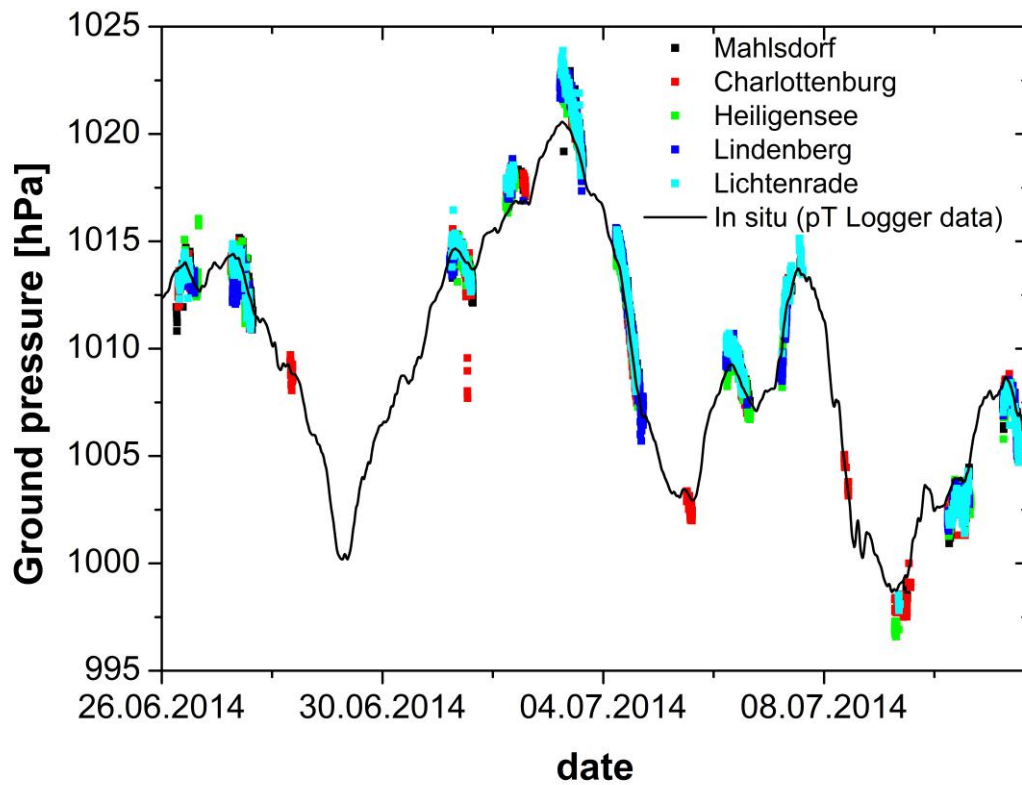
2 Figure 1. Map showing the measurement stations around Berlin

3



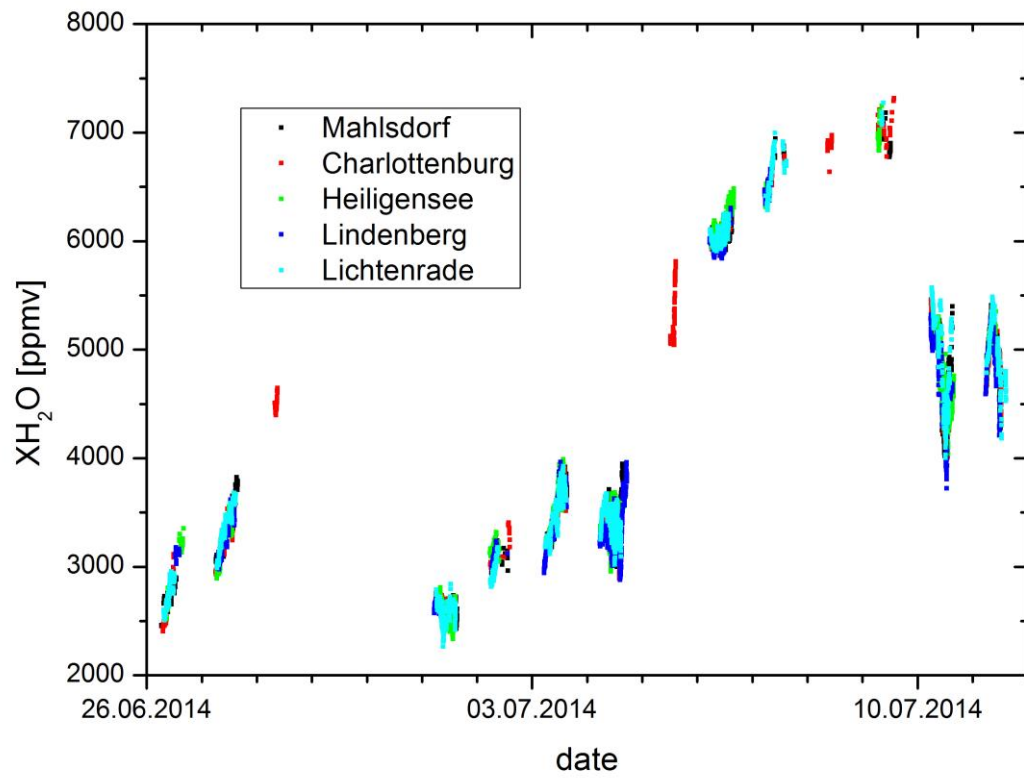
1  
2 Figure 2. The development of the boundary layer thickness during June, 27 according to  
3 ceilometer measurements performed by IMK-IFU in Berlin-Neukölln.

4  
5



1  
2  
3  
4  
5  
6  
7  
8  
9

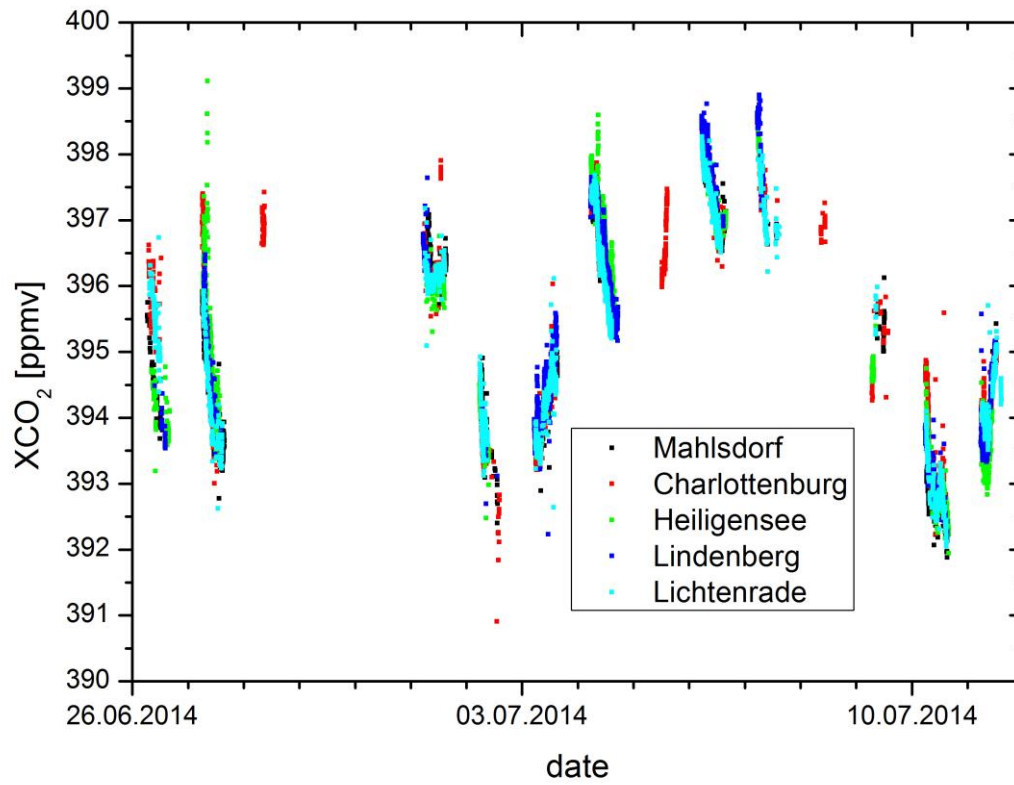
Figure 3. Time series of ground pressure according to the barometer measurements performed at each site (black line) and derived from the infrared spectra (dots). All pressure values were reduced to a common reference altitude of 30 m. For the spectroscopic results, the dry ground pressure has been derived from the 1.27  $\mu\text{m}$  oxygen band and the contribution of water vapour to the total ground pressure has been taken into account. In order to achieve the best agreement with the barometer results, a calibration factor of 0.9713 has been applied to the spectroscopic results.



1

2 Figure 4. Evolution of XH<sub>2</sub>O as measured at all sites during the campaign.

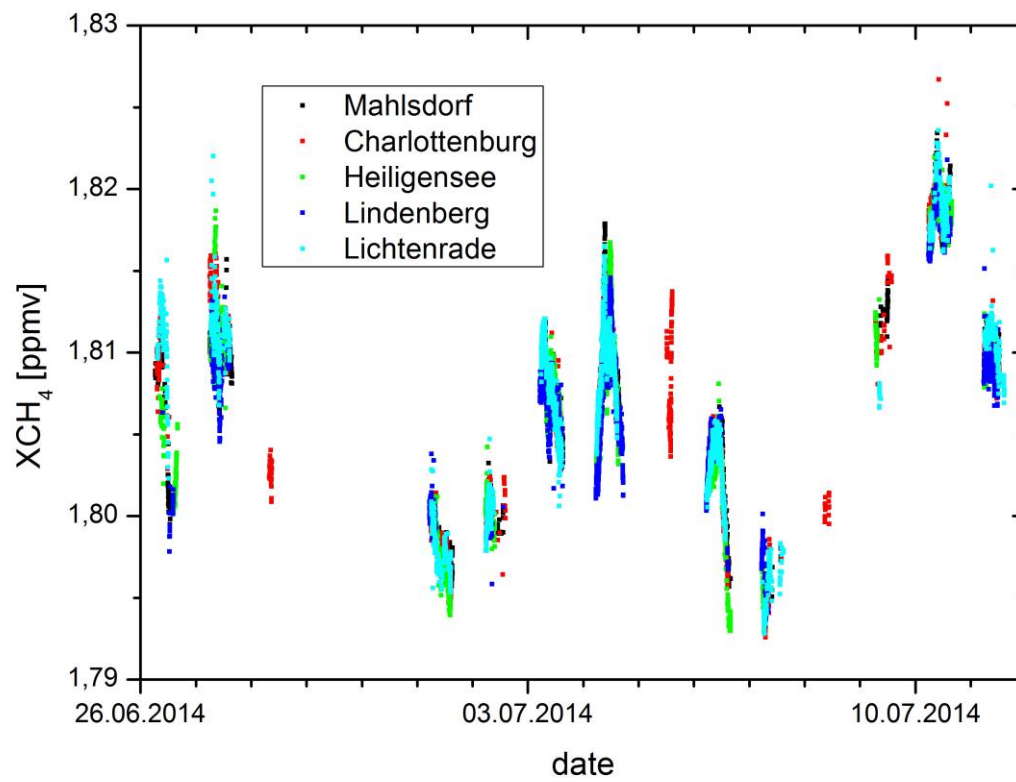
3



1

2 Figure 5. Evolution of XCO<sub>2</sub> as measured at all sites during the campaign.

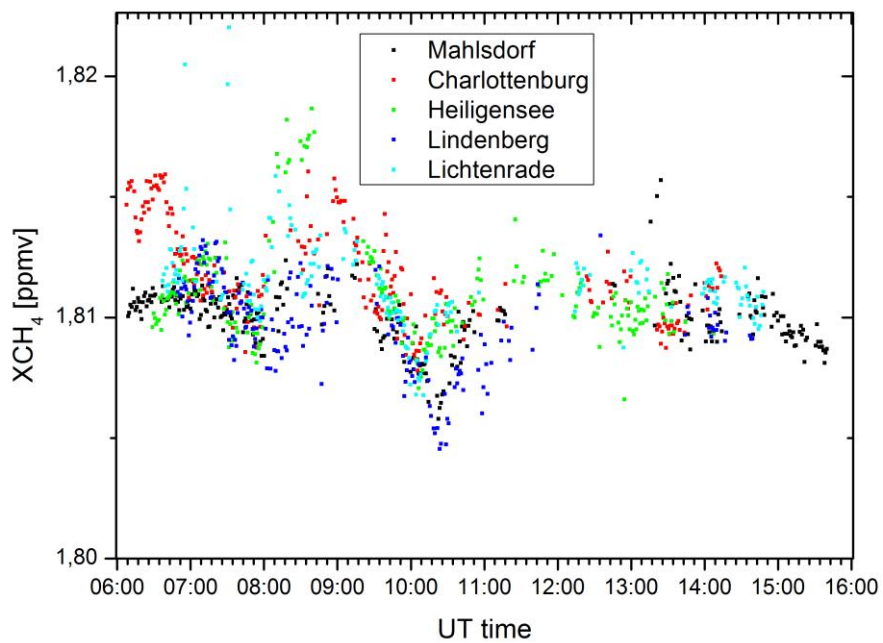
3



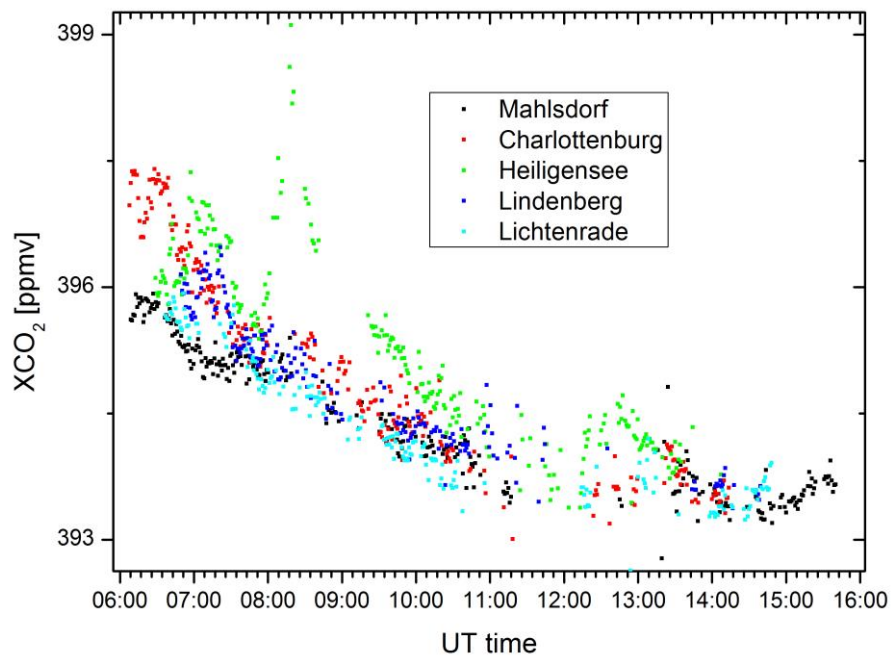
1

2 Figure 6. Evolution of XCH<sub>4</sub> as measured at all sites during the campaign.

3



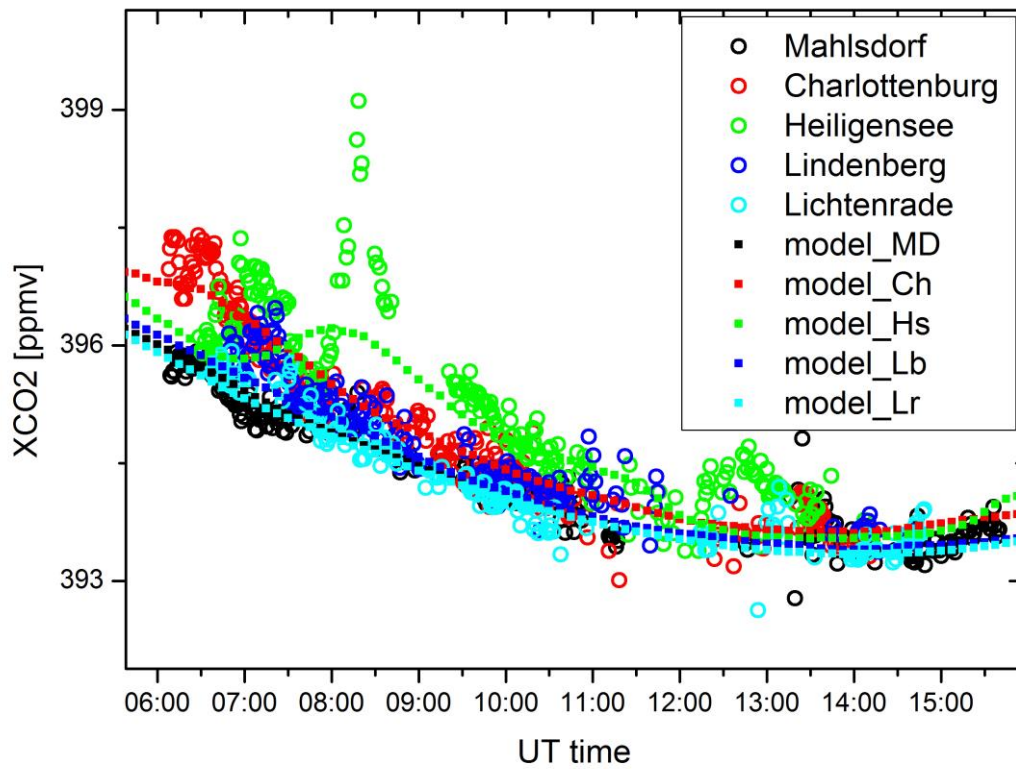
1



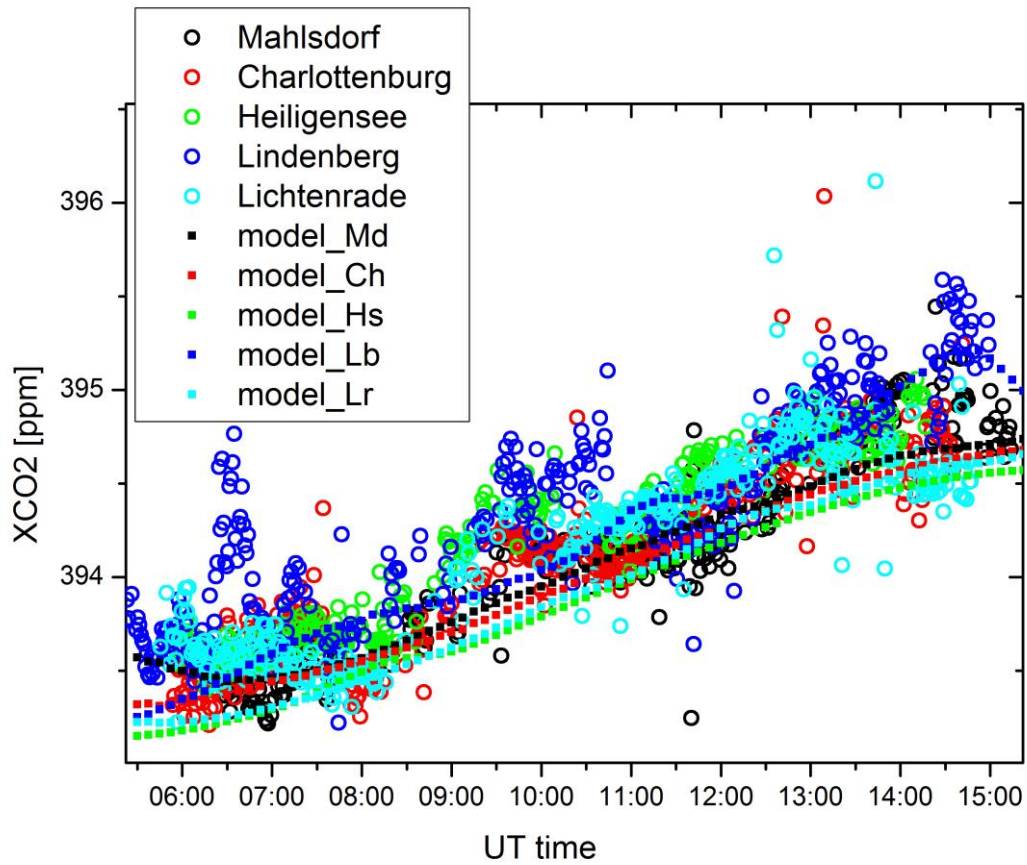
2

3 Figure 7. Observed variability of  $XCH_4$  and  $XCO_2$  during 2014-June-27.

4



1  
 2 Figure 8. Observed and modelled XCO<sub>2</sub> for June, 27. The model enhancements are shown  
 3 superimposed on a smooth polynomial background which has been derived from the  
 4 observations of the upstream stations.  
 5

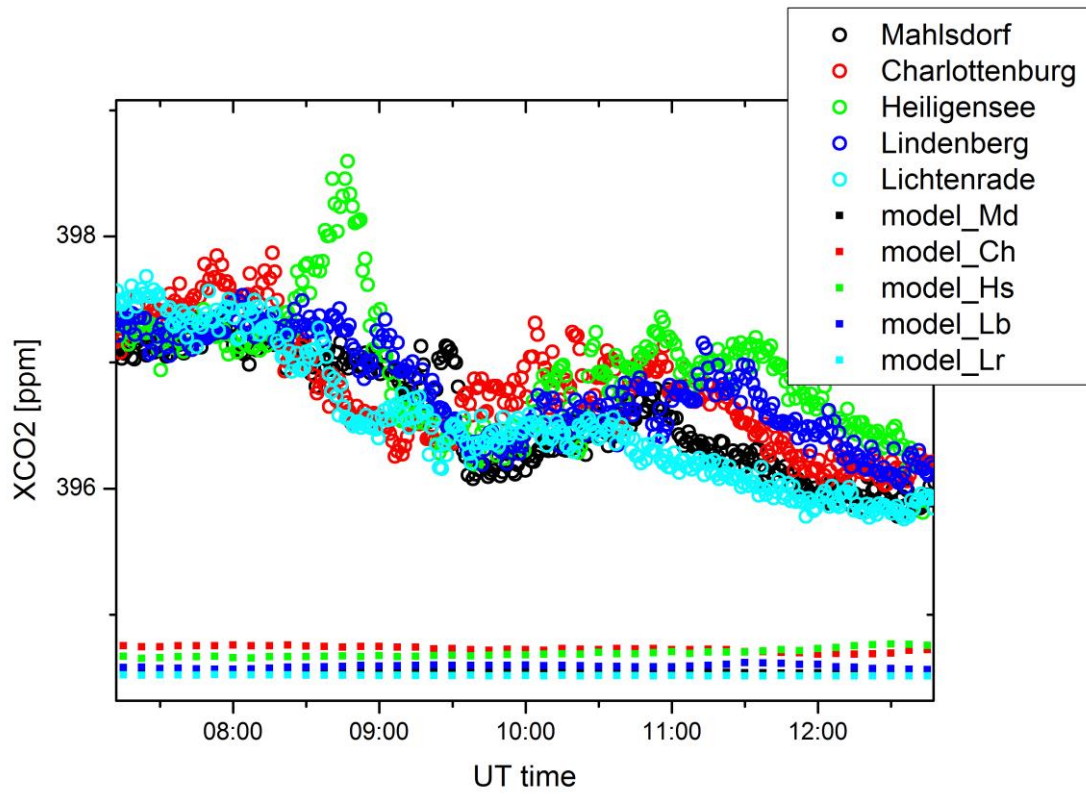


1

2 Figure 9. Observed and modelled XCO2 for July, 3. The model enhancements are shown  
3 superimposed on a smooth polynomial background which has been derived from the  
4 observations of the upstream stations.

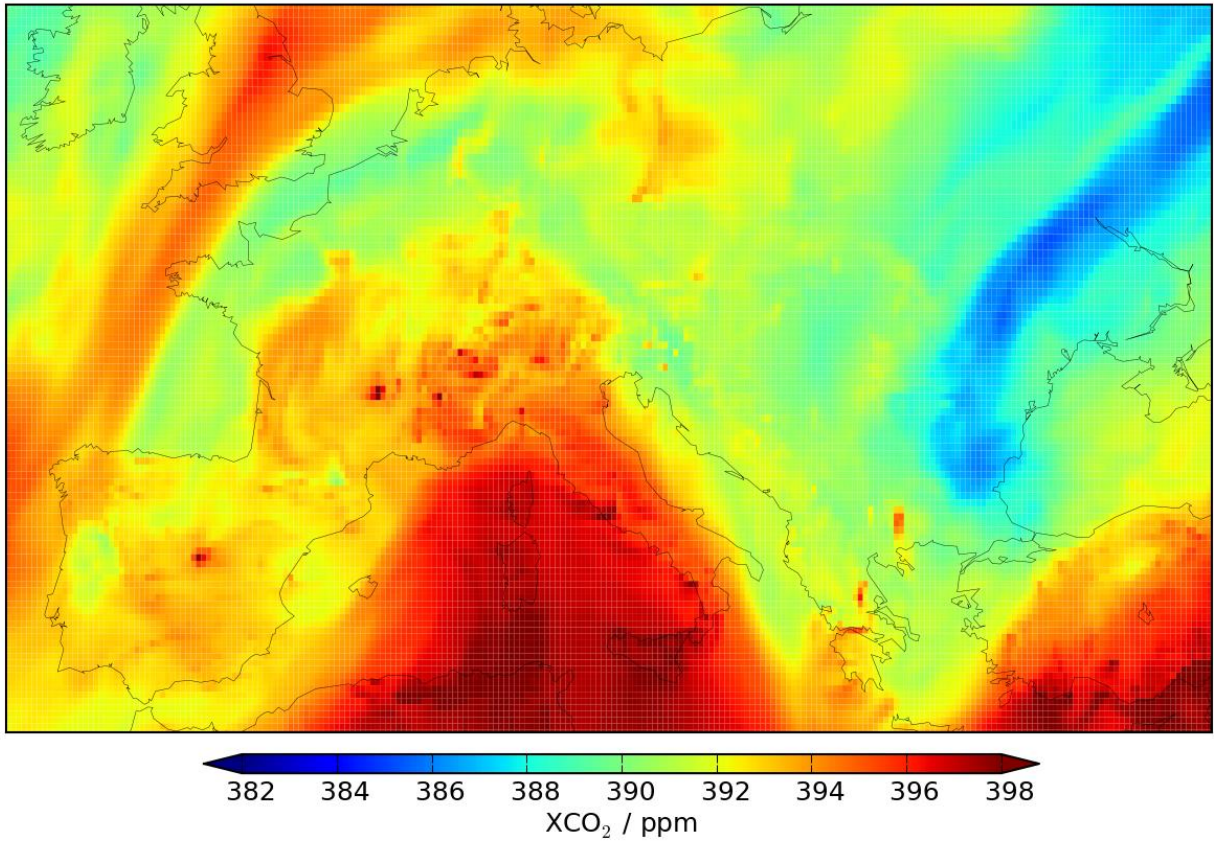
5

6



1  
 2 Figure 10. Observed and modelled XCO<sub>2</sub> for July, 4. Due to the high variability of the  
 3 upstream values observed during this day, no attempt has been made of constructing a  
 4 common background value.  
 5

2014-07-04 06 UT



- 1
- 2 Figure 11. XCO<sub>2</sub> distribution according to the MACC model across central Europe for the
- 3 morning of July, 4. North is up, as orientation marks the continental coastlines are
- 4 superimposed (dark lines).
- 5